Journal of Fluids and Structures 98 (2020) 103113

Contents lists available at ScienceDirect

Journal of Fluids and Structures

journal homepage: www.elsevier.com/locate/jfs

Nonlinear steady states of hyperelastic membrane tubes conveying a viscous non-Newtonian fluid

Vasily Vedeneev

Lomonosov Moscow State University, 1, Leninskie Gory, Moscow, Russia

ARTICLE INFO

Article history:
Received 25 April 2020
Received in revised form 11 July 2020
Accepted 22 July 2020
Available online xxxx

Keywords:
Tubes conveying fluid
Solitary wave
Hyperelastic material
Non-Newtonian fluid

ABSTRACT

We study possible steady states of an infinitely long tube made of a hyperelastic membrane and conveying either an inviscid, or a viscous fluid with power-law rheology. The tube model is geometrically and physically nonlinear; the fluid model is limited to smooth changes in the tube's radius. For the inviscid case, we analyse the tube's stretch and flow velocity range at which standing solitary waves of both the swelling and the necking type exist. For the viscous case, we first analyse the tube's upstream and downstream limit states that are balanced by infinitely growing upstream (and decreasing downstream) fluid pressure and axial stress caused by fluid viscosity. Then we investigate conditions that can connect these limit states by a single solution. We show that such a solution exists only for sufficiently small flow speeds and that it has a form of a kink wave; solitary waves do not exist. For the case of a semi-infinite tube (infinite either upstream or downstream), there exist both kink and solitary wave solutions. For finite-length tubes, there exist solutions of any kind, i.e. in the form of pieces of kink waves, solitary waves, and periodic waves.

1. Introduction

Nonlinear waves in fluid-filled elastic tubes play an important role in problems of the cardiovascular system (Pedley, 2003; Cao et al., 2019). Solitary wave solutions are used for the analysis of pulse waves as well as for the study of the formation of aneurysms (Alhayani et al., 2014; de Gelidia and Bucchia, 2019; Dehghani et al., 2019). In connection with solitary waves, several experimental studies of bulge formation and propagation in elastic tubes have been conducted (Kyriakides and Chang, 1991; Pamplona et al., 2006; Guo et al., 2014; Wang et al., 2019). Theoretical analysis of nonlinear solitary waves in fluid-filled elastic tubes was initially performed with a number of simplified assumptions, such as neglecting axial displacement, weakly nonlinear waves, and a long-wave approximation (Yomosa, 1987; Demiray, 1996), in applications to pulsatile blood flow in arteries. However, it was shown by Epstein and Johnston (2001) that the exact equations of motion for a hyperelastic membrane tube conveying an inviscid fluid have two first integrals and, consequently, can be analysed directly without any additional assumptions. In particular, the existence of solitary waves was proved analytically for the exact membrane tube model. Using the exact model, Fu et al. (2008) studied steady solitary waves for different models of hyperelastic tube material. The relation between the approximate and exact formulations and between the corresponding weakly and fully nonlinear solitary waves was established by Fu and Il'ichev (2010).

The bifurcation diagram shows that a travelling solitary wave separates at zero amplitude from a linear wave that has a finite travelling speed (Il'ichev et al., 2020). When the solitary wave amplitude grows, its travelling speed decreases,

E-mail address: vasily@vedeneev.ru.
URL: http://www.vedeneev.ru.

https://doi.org/10.1016/j.jfluidstructs.2020.103113
0889-9746/

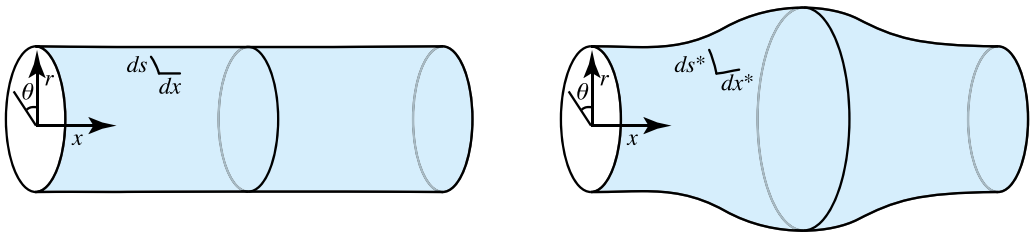

Fig. 1. Cylindrical membrane tube in the initial and the deformed state.

and the solitary wave branch ends, depending on the material model and properties, as either a standing solitary wave (i.e. a static localised bulge) or a kink wave (Il'ichev et al., 2020). A standing solitary wave solution can be considered to be a mathematical model of aneurysm in a blood vessel. As a more adequate description of aneurysm formation, an initial localised wall thinning was introduced into the tube model in the studies of Fu and Xie (2012) and Il'ichev and Fu (2014), where bulged solutions and their stability were analysed. It was shown that there are two types of bulged tube states, one with a smaller and one with a larger amplitude. For the vanishing tube imperfection, the first state tends to a uniform tube, while the second state tends to a standing solitary wave. It was shown that the first state is stable, while the second state is not. However, the presence of a fluid flow stabilises the standing solitary wave (Il'ichev and Fu, 2012; Fu and Il'ichev, 2015) so that both solutions can be stable. In this series of studies, the membrane tube was modelled by an exact, geometrically and physically nonlinear model, but the fluid model was simplistic, with the fluid assumed to be inviscid with a constant velocity distribution in each cross-section. With respect to biomechanical applications, the tube model also had several limitations. First, actual blood vessel properties (Amabili et al., 2020) are anisotropic so that hyperelastic blood vessel models should include an anisotropic part (Vassilevski et al., 2015; Breslavsky et al., 2016). Next, blood vessel walls are sufficiently thick so that their bending stiffness and corresponding shell effects (studied, e.g., by Karagiozis et al., 2007) can be important. Finally, axisymmetry of deformations was assumed, which is not always the case in the cardiovascular system. Nevertheless, this series of studies is an important step towards understanding the nonlinear dynamics of real blood vessels.

Another type of studies, that of fluid flow in collapsible tubes (Grotberg and Jensen, 2004; Heil and Hazel, 2011), deals with viscous fluids, but the tube model, in its 1-dimensional formulation, is either linear or extremely simplified nonlinear in the form of the 'tube law' (Jensen and Pedley, 1989; Jensen, 1990; Pedley and Luo, 1998; Whittaker et al., 2010). Although they are more advanced in terms of fluid mechanics, this type of models does not admit of a bifurcation of a uniform tube to a bulged solitary wave solution. Also, all studies of collapsible tubes consider Newtonian fluid flows; however, it is known that blood in small vessels has essentially non-Newtonian rheology (Moore et al., 1985; Ku, 1997; Gijsen et al., 1999; Anand and Rajagopal, 2004; Galdi et al., 2008). Yushutin (2012) improved the 1-dimensional fluid model to include non-Newtonian power-law rheology, which was used for the analysis of steady states (Poroshina and Vedeneev, 2018) and stability (Vedeneev and Poroshina, 2018) of linearly elastic tubes conveying fluid, under the assumption of long-wave and low-frequency motions.

The goal of the present paper is to combine the two approaches used in the two series of studies, to analyse a geometrically and physically nonlinear hyperelastic membrane tube conveying a viscous non-Newtonian fluid. In Section 2, we upgrade the exact tube model of Epstein and Johnston (2001) by including non-Newtonian fluid viscosity under the assumptions of Yushutin (2012). The rest of the paper deals with steady-state solutions of this system. In Section 3, we analyse the first integrals of the system of equations and introduce the phase plane used in the subsequent analysis. Section 4 is devoted to solitary wave analysis, including a non-constant cross-section velocity distribution but neglecting fluid viscosity. In Section 5, we include fluid viscosity in the analysis. We prove that for the Gent tube material and sufficiently small fluid velocities, there exists a unique steady-steady solution for an infinitely long tube, of which the tube radius changes monotonically so that no solitary waves are possible. For semi-infinite tubes (infinite either upstream or downstream), a second solitary wave solution exists. For finite-length tubes, several solitary wave, periodic wave, and monotonic solutions exist. Section 6 summarises the results and concludes the paper.

2. Equations of motion of an elastic tube containing a flowing viscous fluid

2.1. Formulation of the problem and preliminary relationships

We consider a cylindrical membrane tube with a circular cross-section with a thickness of h and a radius of R, made of hyperelastic material (Fig. 1). The ratio h/R is sufficiently small for the bending stresses to be neglected compared to the membrane stresses. The tube conveys a non-Newtonian viscous fluid whose rheology obeys a power law. We restrict ourselves to axisymmetric motion with two components of the displacement vector, longitudinal (axial) u and radial w.

Epstein and Johnston (2001) gave a self-contained derivation of the exact equations of motion for the case of an inviscid fluid. Here we briefly revisit this derivation to take fluid viscosity and rheology into consideration. The equations of motion

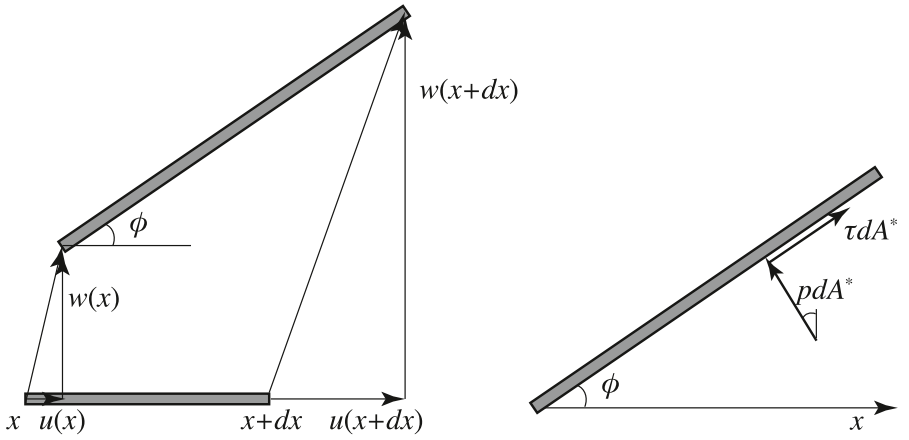

Fig. 2. The undeformed dx and the deformed dx^* element of the tube (a); fluid forces (b).

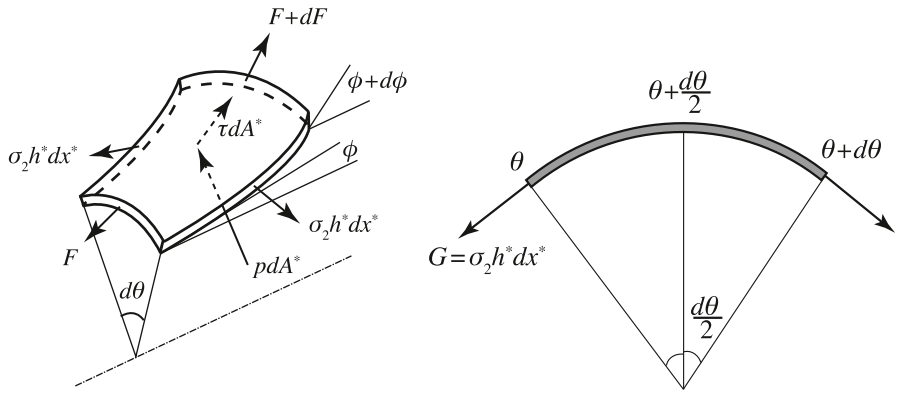

Fig. 3. Forces acting on a deformed shell element.

are derived in Lagrangian cylindrical coordinates corresponding to the undeformed state of the tube. The x axis is directed along the tube's axis, and the angle θ is the circumferential direction. The axial and circumferential length elements are denoted by dx and ds; the area element is $dA = dxds$ (Fig. 1). In the deformed state, the lengths and area of the same elements, as well as other values, will be denoted by a star.

In what follows, we will need a relationship between the length of the element dx before and after deformation and the angle φ between them. From Fig. 2a we have

$$dx^* = \sqrt{(1+u')^2 + w'^2}dx, \quad \varphi = \arctan\left(\frac{w'}{1+u'}\right),$$

where the prime denotes differentiation with respect to the Lagrangian coordinate x. The lengths of the element ds and the sizes of the area dA before and after deformation are related as

$$ds^* = \left(1+\frac{w}{R}\right)ds, \quad dA^* = \sqrt{(1+u')^2 + w'^2}\left(1+\frac{w}{R}\right)dA.$$

2.2. Equations of the tube motion

Consider fluid forces acting in the axial direction on a tube element with an undeformed area dA (Figs. 2b, 3a). After simple algebra, for pressure and friction forces we have

$$-p\,\sin\varphi\,dA^* = -pw'\left(1+\frac{w}{R}\right)dA, \quad \tau\cos\varphi dA^* = \tau\left(1+u'\right)\left(1+\frac{w}{R}\right)dA.$$

The force resulting from elastic tensile stress (Fig. 3a) is expressed as follows:

$$F(x+dx)\cos(\varphi+d\varphi) - F(x)\cos\varphi = \left(\frac{\sigma_1 h^*(1+w/R)}{\sqrt{(1+u')^2+w'^2}}(1+u')\right)' dA,$$

where $F = \sigma_1 h^* ds^*$ and σ_1 is the longitudinal physical component of Cauchy stress. Here we assumed a uniform distribution of stresses over the tube thickness, which corresponds to the membrane model.

Balancing these forces with the inertial force $\rho^* h^* \ddot{u} dA^* = \rho h \ddot{u} dA$, where ρ is the material density, we obtain the longitudinal equation of motion:

$$\rho h \ddot{u} = -p w' \left(1 + \frac{w}{R}\right) + \tau (1 + u') \left(1 + \frac{w}{R}\right) + \left(\frac{\sigma_1 h^* (1 + w/R)}{\sqrt{(1+u')^2 + w'^2}} (1 + u') \right)'. \tag{1}$$

Similarly, for fluid forces acting in the radial direction (Figs. 2b, 3a), we obtain

$$p \cos\varphi \, dA^* = p(1 + u') \left(1 + \frac{w}{R}\right) dA, \quad \tau \sin\varphi dA^* = \tau w' \left(1 + \frac{w}{R}\right) dA.$$

The radial force from elastic stresses is the sum of the longitudinal stress at ends x and $x + dx$ (Fig. 3a),

$$F(x + dx) \sin(\varphi + d\varphi) - F(x) \sin\varphi = \left(\sigma_1 h^* (1 + w/R) \frac{w'}{\sqrt{(1+u')^2 + w'^2}} \right)' dA,$$

and the circumferential stress at ends s and $s + ds$ (Fig. 3b),

$$-G(\theta + d\theta) \sin(d\theta/2) - G(\theta) \sin(d\theta/2) = -\sigma_2 h^* \frac{\sqrt{(1+u')^2 + w'^2}}{R} dA,$$

where σ_2 is the circumferential physical component of the Cauchy stress.

Balancing the radial elastic and fluid forces with the inertial force $\rho^* h^* dA^* \ddot{w} = \rho h dA \ddot{w}$, we obtain the radial equation of motion:

$$\begin{aligned} \rho h \ddot{w} = {} & p(1 + u') \left(1 + \frac{w}{R}\right) + \tau w' \left(1 + \frac{w}{R}\right) + \\ & \left(\sigma_1 h^* (1 + w/R) \frac{w'}{\sqrt{(1+u')^2 + w'^2}} \right)' - \sigma_2 h^* \frac{\sqrt{(1+u')^2 + w'^2}}{R}. \end{aligned} \tag{2}$$

2.3. Equations of fluid motion

Next, we consider the motion of the fluid. We will assume that its rheology obeys the Ostwald–de Waele power law, which for pure shear reads

$$\tau^{12} = \mu \left(\frac{dv_1}{dx_2} \right)^n$$

and for the general case is

$$\tau^{ij} = 2\mu \left(\sqrt{2} I_2(e) \right)^{n-1} e^{ij}, \qquad I_2 = \sqrt{e_{ij} e^{ij}}, \tag{3}$$

where τ^{ij} and e^{ij} are the components of the viscous stress tensor and strain rate tensor. The special case of $n = 1$ corresponds to a Newtonian viscous fluid, and $\mu = 0$ corresponds to an ideal fluid.

Assuming that the motion is slow (quasi-stationary) and that the wavelengths are large, a Poiseuille velocity distribution is established in each tube cross-section at each moment:

$$v_x(x, r) = v_f(x) \frac{3n + 1}{n + 1} \left(1 - \left(\frac{r}{R + w} \right)^{\frac{n+1}{n}} \right), \tag{4}$$

where $v_f(x)$ is the average velocity in the section. Under this assumption, the Navier–Stokes equations integrated over the cross-section give a spatially one-dimensional system of equations, as shown by Yushutin (2012). A different form of this system was obtained by Vedeneev and Poroshina (2018); equations (2.10) and (2.11) of their paper in the present notations have the form

$$\begin{aligned} & \frac{\partial w}{\partial t} + v_f \frac{\partial w}{\partial q} + \frac{R + w}{2} \frac{\partial v_f}{\partial q} = 0, \\ & \frac{\partial v_f}{\partial t} + \frac{3n + 1}{2n + 1} v_f \frac{\partial v_f}{\partial q} - \frac{2n}{2n + 1} \frac{v_f}{R + w} \frac{\partial w}{\partial t} + \frac{1}{\rho_f} \frac{\partial p}{\partial q} + \frac{\mu}{\rho_f} \frac{2(3n + 1)^n}{n^n} \frac{v_f^n}{(R + w)^{n+1}} = 0, \end{aligned} \tag{5}$$

where q is the Eulerian coordinate of the tube axis.

To have both tube and fluid equations formulated in the same coordinate system, we now switch to Lagrangian coordinates in the fluid equations (5). The transformation from Eulerian to Lagrangian coordinates is expressed as

$$\frac{\partial f}{\partial q} = \frac{f'}{1 + u'}, \qquad \frac{\partial f}{\partial t} = \dot{f} - f' \frac{\dot{u}}{1 + u'}$$

for any function f. Substituting these into system (5), and slightly transforming the resulting equations, we obtain

$$\dot{w} + \dot{w}u' - w'\dot{u} + v_f w' + \frac{1}{2}(R+w)v_f' = 0, \tag{6}$$

$$\rho_f \left(\dot{v}_f + \dot{v}_f u' - v_f'\dot{u} + \frac{3n+1}{2n+1} v_f v_f' - \frac{2n}{2n+1}\frac{v_f}{R+w}\left(\dot{w} + \dot{w}u' - w'\dot{u}\right)\right) +$$
$$+ p' + \mu \frac{2(3n+1)^n}{n^n} \frac{v_f^n}{(R+w)^{n+1}}(1+u') = 0. \tag{7}$$

2.4. Expression for viscous friction τ

To close the system, let us obtain an expression for the viscous friction τ included in the equations of the tube motion. For the Poiseuille velocity distribution (4), the wall friction comes only from the component $\tau = \tau_{rx}$, which is expressed as

$$\tau = \mu \left(\frac{\partial v_x}{\partial r} \right)^n.$$

Using the distribution (4), we obtain the friction at the tube wall

$$\tau(x,t) = \mu \left(\frac{v_f(x,t)}{R + w(x,t)} \right)^n \left(\frac{1+3n}{n} \right)^n. \tag{8}$$

2.5. Closed system of equations

Hereunder we will assume the incompressibility of the tube material, which excludes the deformed thickness from Eqs. (1) and (2):

$$h^* = \frac{h}{\sqrt{(1+u')^2 + w'^2}(1 + w/R)}. \tag{9}$$

Then the system consisting of Eqs. (1), (2), (6), (7), and (8), supplemented by a hyperelastic model of the tube's material, is a closed system of equations based on the geometrically and physically nonlinear theory of the membrane tube (Epstein and Johnston, 2001) and the approximate one-dimensional equations of motion of a power-law fluid derived under the assumptions of Yushutin (2012) and Vedeneev and Poroshina (2018). Thus, this system generalises both the equations of Epstein and Johnston (2001) by taking into account the viscosity and rheology of the fluid and the equations of Yushutin (2012) and Vedeneev and Poroshina (2018) by taking into account the geometric and physical nonlinearity of the tube. In particular, for $n = 0$ (a uniform velocity profile) and $\mu = 0$ (an inviscid fluid), the system of equations coincides with the system of Epstein and Johnston (2001).

3. Steady-state equations

Next, we will study the possible steady states of the tube conveying fluid, by setting all time derivatives equal to zero. Then the system consisting of Eqs. (1), (2), (6), and (7), taking into account equation (9), will take the form

$$-pw'\left(1 + \frac{w}{R}\right) + \tau(1+u_s)\left(1+\frac{w}{R}\right) + \left(\frac{\sigma_1 h}{(1+u_s)^2 + w'^2}(1+u_s)\right)' = 0, \tag{10}$$

$$p(1+u_s)\left(1+\frac{w}{R}\right) + \tau w'\left(1+\frac{w}{R}\right) + \left(\sigma_1 h \frac{w'}{(1+u_s)^2 + w'^2}\right)' - \frac{\sigma_2 h}{R+w} = 0, \tag{11}$$

$$v_f w' + \frac{1}{2}(R+w)v_f' = 0, \tag{12}$$

$$\rho_f \frac{3n+1}{2n+1} v_f v_f' + p' + \frac{2\tau}{R+w}(1+u_s) = 0, \tag{13}$$

where $u_s(x) \equiv u'(x)$ (the function $u(x)$ itself is not present in the steady-state equations).

3.1. Integration of the fluid equations

Note that Eq. (12) is integrated and gives the relationship between fluid velocity and radial displacement (conservation of fluid mass):

$$v_f(w) = v_{f0}\frac{(R+w_0)^2}{(R+w)^2}.$$

With the use of this relationship, Eq. (13) is also integrated in the absence of viscosity (generalised Bernoulli equation):

$$p_{inv}(w) = p_0 + \rho_f \frac{3n+1}{2n+1}\frac{v_{f0}^2}{2}\left(1 - \left(\frac{R+w_0}{R+w}\right)^4\right).$$

In the presence of viscosity, the pressure takes the form

$$p(x) = p_{inv}(x) + f(x), \qquad f(x) = -\int_{x_0}^{x} \frac{2\tau}{R+w}(1+u_s)dx, \tag{14}$$

where $f(x)$ is a monotonically decreasing function reflecting viscous pressure loss.

3.2. First integrals of the tube equations

Let us now consider equations (10) and (11). It is known that for an inviscid fluid, they have two first integrals (Epstein and Johnston, 2001; Fu and Il'ichev, 2010). Let us denote the principal (axial and circumferential) stretches:

$$\lambda_1 = \sqrt{(1+u_s)^2 + w'^2}, \quad \lambda_2 = 1 + \frac{w}{R}.$$

Then these equations can be rewritten in the form

$$\left(\frac{\sigma_1}{\lambda_1^2}(1+u_s)\right)' - p\frac{R}{h}\lambda_2\lambda_2' + \frac{\tau}{h}(1+u_s)\lambda_2 = 0, \tag{15}$$

$$\left(\sigma_1\frac{\lambda_2'}{\lambda_1^2}\right)' - \frac{\sigma_2}{R^2\lambda_2} + p\frac{1}{Rh}(1+u_s)\lambda_2 + \frac{\tau}{h}\lambda_2'\lambda_2 = 0, \tag{16}$$

$$p = p_{inv} + f, \qquad p_{inv} = p_0 + \rho_f\frac{3n+1}{2n+1}\frac{v_{f0}^2}{2}\left(1 - \left(\frac{\lambda_{20}}{\lambda_2}\right)^4\right).$$

Note that hereunder, we use the notations of Epstein and Johnston (2001) for the principal stretches, which differ from the notations of Fu and Il'ichev (2010) in that the axial and circumferential stretches are switched.

Next, we define a hyperelastic material model that for the incompressible case reads

$$\sigma_i = \lambda_i W_i, \quad W_i = \frac{\partial W}{\partial \lambda_i}, \quad i = 1, 2,$$

where $W(\lambda_1, \lambda_2) = \hat{W}(\lambda_1, \lambda_2, (\lambda_1\lambda_2)^{-1})$ and $\hat{W}(\lambda_1, \lambda_2, \lambda_3)$ is the strain energy function (see Fu et al., 2008 for details).

Representing the pressure in the form of the sum of 'inviscid' pressure p_{inv} and the viscous pressure loss f, we integrate equation (15) and obtain

$$\frac{W_1}{\lambda_1}(1+u_s) - p_0\frac{R}{h}\frac{\lambda_2^2}{2} - \rho_f\frac{R}{h}\frac{3n+1}{2n+1}\frac{v_{f0}^2}{4}\lambda_2^2\left(1 + \left(\frac{\lambda_{20}}{\lambda_2}\right)^4\right) = C_1(x) + F(x),$$

$$C_1(x) = -\int_{x_0}^{x}\frac{\tau}{h}(1+u_s)\lambda_2 dx, \qquad F(x) = \int_{x_0}^{x} f\frac{R}{h}\lambda_2\lambda_2' dx.$$

Let us consider in more detail the behaviour of $F(x)$, integrating by parts:

$$F(x) = \int f\frac{R}{h}\frac{d}{dx}\left(\frac{\lambda_2^2}{2}\right)dx = f\frac{R}{h}\frac{\lambda_2^2}{2} - \int f'\frac{R}{h}\frac{\lambda_2^2}{2}dx = f\frac{R}{h}\frac{\lambda_2^2}{2} + \int\frac{\tau}{h}(1+u_s)\lambda_2 dx.$$

It is seen that the first term can be combined with p_0 on the left-hand side, and the second (integral) term is cancelled by the same term in $C_1(x)$. Finally, we get

$$\frac{W_1}{\lambda_1}(1+u_s) - p_0(x)\frac{R}{h}\frac{\lambda_2^2}{2} - \rho_f\frac{R}{h}\frac{3n+1}{2n+1}\frac{v_{f0}^2}{4}\lambda_2^2\left(1 + \left(\frac{\lambda_{20}}{\lambda_2}\right)^4\right) = C_1, \tag{17}$$

where $C_1 = \text{const}$. Hence, the effect of viscous friction consists of a monotonic pressure decrease, $p_0(x) = p_0 + f(x)$, due to friction losses $f(x)$.

To derive the other first integral, consider the sum of Eq. (15) multiplied by $(1+u_s)$ and Eq. (16) multiplied by $R^2\lambda_2'$:

$$\left(\frac{\sigma_1}{\lambda_1^2}(1+u_s)\right)'(1+u_s) + \left(\sigma_1\frac{\lambda_2'}{\lambda_1^2}\right)'R^2\lambda_2' - \frac{\sigma_2\lambda_2'}{\lambda_2} = -\frac{\tau}{h}(1+u_s)^2\lambda_2 - \frac{\tau}{h}R^2\lambda_2'^2\lambda_2.$$

After simple algebra, the resulting equation is rewritten as

$$\sigma_1' - W' = -\frac{\tau}{h}\lambda_1^2\lambda_2.$$

Integrating, we get

$$W - \sigma_1 = C_2(x), \qquad C_2(x) = \int_{x_1}^{x} \frac{\tau}{h}\lambda_1^2\lambda_2 dx, \tag{18}$$

where $C_2(x)$ is a monotonously growing function.

In the absence of friction, $p_0(x) = \text{const}$, $C_2(x) = \text{const}$, and expressions (17) and (18) are the first integrals. In the presence of friction, $p_0(x)$ is a monotonously decreasing function, and $C_2(x)$ is a monotonously increasing function; moreover, they themselves depend on the solution. Strictly speaking, expressions (17) and (18) are no longer the first integrals, but we will call them so for brevity.

Both first integrals (17) and (18) have a clear physical meaning. Eq. (17) reflects the conservation of the resultant force in the axial direction at each cross-section. Eq. (18) is the equilibrium equation of a membrane element, in projection onto the deformed element; in particular, fluid pressure is not present in Eq. (18), because it is cancelled at the projection. Note that the fluid friction acts separately in these equations: only through pressure losses in Eq. (17) and only through increasing upstream (and decreasing downstream) traction force in Eq. (18).

3.3. Non-dimensionalisation and transition to variables λ_1 and λ_2

We proceed to dimensionless quantities by choosing the non-deformed tube radius R as the length scale, the shear modulus of the tube material G as the stress scale, and the fluid density ρ_f as the density scale. In addition, to get rid of the factors R/h, for pressure p and friction τ we choose the scale $P = Gh/R$, and for the fluid speed v_f the scale $\sqrt{P/\rho_f}$. Also, we switch from the unknowns $u_s(x)$ and $w(x)$ to the principal stretches $\lambda_1(x)$ and $\lambda_2(x)$, which have the dimensionless form

$$\lambda_1 = \sqrt{(1+u_s)^2 + w'^2}, \quad \lambda_2 = 1 + w.$$

Expressing u_s and w through λ_1 and λ_2, the first integrals can be rewritten in the form

$$\lambda_2' = \lambda_1 \sqrt{1 - \frac{1}{W_1(\lambda_1,\lambda_2)^2}\left(p_0(x)\frac{\lambda_2^2}{2} + \frac{3n+1}{2n+1}\frac{v_{f0}^2}{4}\lambda_2^2\left(1 + \left(\frac{\lambda_{20}}{\lambda_2}\right)^4\right) + C_1\right)^2}, \tag{19}$$

$$W(\lambda_1,\lambda_2) - \lambda_1 W_1(\lambda_1,\lambda_2) = C_2(x). \tag{20}$$

Expression (20) is the algebraic relationship between λ_1, λ_2, and x. If $C_2(x)$ is known, then from this expression we find implicitly $\lambda_1 = \lambda_1(\lambda_2, C_2(x))$. Substituting into Eq. (19), we obtain an ordinary differential equation for the function $\lambda_2(x)$.

To simplify the non-dimensional expression (8) for the friction, we introduce the Reynolds number of the power-law fluid in the definition of Metzner and Reed (1955):

$$\mathrm{Re} = \frac{\rho_f (R+w)^n v_f^{2-n}}{\mu}\frac{8n^n}{(3n+1)^n}.$$

Then the expression for dimensionless friction is written as

$$\tau = \frac{8v_f^2}{\mathrm{Re}}. \tag{21}$$

Here, both the dimensionless average velocity v_f and the Reynolds–Metzner–Reed number Re are not constants; i.e. they are functions of x.

3.4. Phase plane

To study the possible types of solutions, it is useful to increase the order of the differential equation (19) to the second order, thus getting rid of C_1, and to investigate the phase plane of the resulting equation, as in Poroshina and Vedeneev (2018). Differentiating equation (19), we get

$$\lambda_2'' = \frac{\lambda_1'\lambda_2'}{\lambda_1} - \frac{\lambda_1}{\lambda_2' W_1}\left\{\sqrt{\lambda_1^2 - \lambda_2'^2}\left(p_0'\frac{\lambda_2^2}{2} + \lambda_2\lambda_2'\left[p_0 + \frac{3n+1}{2n+1}\frac{v_{f0}^2}{2}\left(1 - \left(\frac{\lambda_{20}}{x}\right)^4\right)\right]\right) - \frac{\lambda_1^2 - \lambda_2'^2}{\lambda_1}W_1'\right\}. \tag{22}$$

To find the expression $\lambda_1'(\lambda_1, \lambda_2, \lambda_2')$, we differentiate equation (20) to obtain

$$\lambda_1' = \lambda_2' \frac{W_2 - \lambda_1 W_{12}}{\lambda_1 W_{11}} - \frac{C_2'}{\lambda_1 W_{11}},$$

where $W_{ij} = \partial^2 W / \partial\lambda_i \partial\lambda_j$. Next, to compute $W_1'(\lambda_1, \lambda_2)$, we write

$$W_1' = W_{11}\lambda_1' + W_{12}\lambda_2' = \lambda_2' \frac{W_2 - \lambda_1 W_{12}}{\lambda_1} - \frac{C_2'}{\lambda_1} + W_{12}\lambda_2' = \frac{\lambda_2'}{\lambda_1} W_2 - \frac{C_2'}{\lambda_1}.$$

Substituting these expressions into Eq. (22) and noting that the term with p_0' is cancelled by the term $-C_2'/\lambda_1$ in the expansion of W_1', we obtain

$$\begin{cases} X' = Y, \\ Y' = -\tau \dfrac{XY}{W_{11}} + Y^2 \dfrac{W_2 - \lambda_1 W_{12}}{\lambda_1^2 W_{11}} - \\ \quad - \dfrac{\lambda_1}{W_1} \left\{ X\sqrt{\lambda_1^2 - Y^2} \left(p_0(x) + \dfrac{3n+1}{2n+1} \dfrac{v_{f0}^2}{2} \left(1 - \left(\dfrac{\lambda_{20}}{X} \right)^4 \right) \right) - \dfrac{\lambda_1^2 - Y^2}{\lambda_1^2} W_2 \right\}. \end{cases} \tag{23}$$

where $X \equiv \lambda_2$, $\lambda_1(X, x)$ is the function obtained by solving algebraic equation (20) for a given value of $C_2(x)$, and the axial Lagrangian coordinate x acts as an analogue of time in a dynamic system.

4. Steady states in the case of an inviscid fluid

In this section, we set $\tau = 0$, i.e. consider an inviscid fluid, but keep a non-constant cross-sectional velocity distribution (4). Therefore, $p_0(x) = \text{const}$, $C_2(x) = \text{const}$, and, consequently, $\lambda_1 = \lambda_1(X)$. We obtain the following autonomous system of equations:

$$\begin{cases} X' = Y, \\ Y' = Y^2 \dfrac{W_2 - \lambda_1 W_{12}}{\lambda_1^2 W_{11}} - \\ \quad - \dfrac{\lambda_1}{W_1} \left\{ X\sqrt{\lambda_1^2 - Y^2} \left(p_0 + \dfrac{3n+1}{2n+1} \dfrac{v_{f0}^2}{2} \left(1 - \left(\dfrac{\lambda_{20}}{X} \right)^4 \right) \right) - \dfrac{\lambda_1^2 - Y^2}{\lambda_1^2} W_2 \right\}. \end{cases} \tag{24}$$

It can immediately be seen that for the inviscid fluid, the non-constant velocity distribution is expressed only in the factor $(3n + 1)/(2n + 1)$, which tends to 1 as $n \to 0$, i.e. as the velocity distribution tends to a constant. Hence, the effect of the cross-sectional velocity distribution consists of increasing the effective mean flow velocity by a factor $\sqrt{(3n+1)/(2n+1)}$ compared to a constant distribution. In particular, for a regular parabolic velocity profile ($n = 1$), the effective velocity is increased by $\approx 15\%$ with respect to the uniform profile.

4.1. Phase-plane structure

As can be seen, the phase plane of Eq. (24) is symmetric about the X axis, is two-sheeted (due to the square root), and is defined only for $|Y| < |\lambda_1(X)|$. We will call the lines $Y = \pm\lambda_1(X)$ the limit lines: they are the transition lines of the integral curves from one sheet of the Riemann surface to the other. It is easy to verify that the limit lines are integral trajectories themselves, but the uniqueness theorem for an integral trajectory passing through a given point is not valid for limit lines. Physically, the points lying on the limit lines correspond to the vertical tangent to the tube surface ($u_s = -1$). In this case, the assumption of flow laminarity inside the tube is not correct: the flow will detach from the walls and switch to a complex unsteady motion. We will call such a situation the tube's collapse; it is obvious that the steady state without collapse corresponds to only one sheet of the phase plane, corresponding to the positive value of the square root. Further, we restrict ourselves to considering this sheet of the phase plane.

The stationary points of the phase plane (X_s, Y_s) are determined by $Y_s = 0$, and X_s are the roots of the equation

$$S(X) = -X \left(p_0 + \frac{3n+1}{2n+1} \frac{v_{f0}^2}{2} \left(1 - \left(\frac{\lambda_{20}}{X} \right)^4 \right) \right) + \frac{W_2(\lambda_1(X), X)}{\lambda_1(X)} = 0. \tag{25}$$

They correspond to possible uniform states of an infinitely long tube. The type of stationary points is determined by the value of $dS(X_s)/dX$: for $W_1 > 0$ (tensile axial stress in the tube wall), they are of a centre type when $dS(X_s)/dX < 0$ and of a saddle type when $dS(X_s)/dX > 0$; for $W_1 < 0$ (compressive axial stress), the types are reversed. The integral curves emerging from the saddle point (separatrices) and returning back to the same point correspond to standing solitary waves.

The phase plane of Eq. (24) is characterised by three parameters: p_0, v_{f0}, and C_2. The parameter C_1 defines only a specific integral curve in the phase plane. To determine the physical meaning of these parameters, we assume that the tube state is homogeneous as $x \to \pm\infty$; i.e. all its parameters tend to constants. This far-field state is characterised

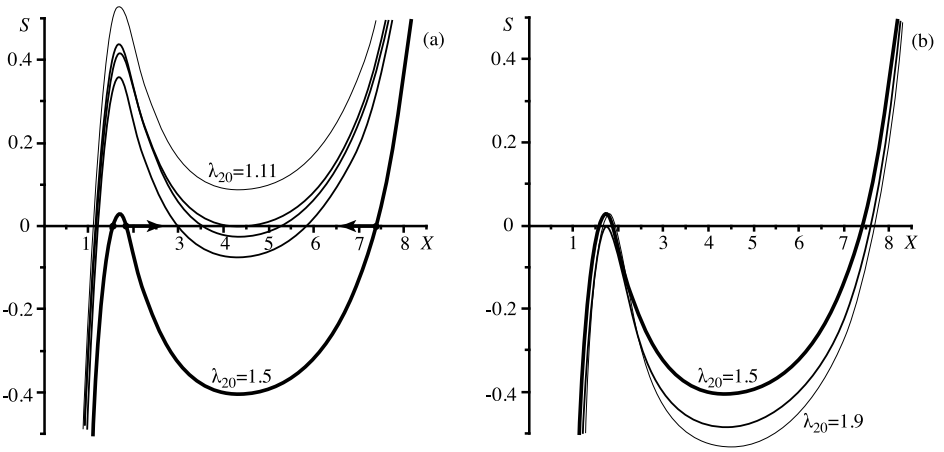

Fig. 4. Plot of the function $S(X)$ for $\lambda_{10} = 1$ and $\lambda_{20} = 1.5$, 1.1763, 1.15, 1.14, 1.11 (a), for $\lambda_{20} = 1.5$, 1.69, 1.9 (b).

by stretches λ_{10} and λ_{20}. After setting these stretches, the constant C_2 and, therefore, the function $\lambda_1(X)$ are uniquely determined from Eq. (20). The fluid pressure p_0 is expressed from the equilibrium condition using Eq. (16):

$$p_0 = \frac{W_2(\lambda_{10}, \lambda_{20})}{\lambda_{10}\lambda_{20}}. \tag{26}$$

The fluid velocity at infinity, v_{f0}, can be set arbitrarily.

4.2. Material model

Since further study without specification of the material model is impossible, we will consider the Gent model of incompressible hyperelastic material (Gent, 1996; Horgan, 2015):

$$W(\lambda_1, \lambda_2) = \hat{W}(\lambda_1, \lambda_2, (\lambda_1\lambda_2)^{-1}), \qquad \hat{W}(\lambda_1, \lambda_2, \lambda_3) = -\frac{1}{2}GJ_m \ln\left(1 - \frac{\lambda_1^2 + \lambda_2^2 + \lambda_3^2 - 3}{J_m}\right),$$

with the shear modulus $G = 10^6$ Pa and $J_m = 97.3$ corresponding to rubber properties. By direct calculations, we find

$$W_i = \frac{\partial W(\lambda_1, \lambda_2)}{\partial \lambda_i} = Ga\left(\lambda_i^2 - (\lambda_1\lambda_2)^{-2}\right)\lambda_i^{-1}, \qquad i = 1, 2,$$

$$W_{11} = \frac{\partial W_1(\lambda_1, \lambda_2)}{\partial \lambda_1} = Ga\left(a\frac{2\lambda_1^{-2}(\lambda_1^2 - (\lambda_1\lambda_2)^{-2})^2}{J_m} + (1 + 3\lambda_1^{-4}\lambda_2^{-2})\right),$$

$$W_{12} = \frac{\partial W_1(\lambda_1, \lambda_2)}{\partial \lambda_2} = Ga\left(a\frac{2(\lambda_1\lambda_2)^{-1}(\lambda_1^2 - (\lambda_1\lambda_2)^{-2})(\lambda_2^2 - (\lambda_1\lambda_2)^{-2})}{J_m} + 2(\lambda_1\lambda_2)^{-3}\right),$$

$$a = \left(1 - \frac{\lambda_1^2 + \lambda_2^2 + (\lambda_1\lambda_2)^{-2} - 3}{J_m}\right)^{-1}.$$

As the Gent material has limited stretch that reflects the limited extensibility of molecular chains, the phase plane is defined for those values of $X \equiv \lambda_2$ for which there is at least one λ_1 such that $a(\lambda_1, \lambda_2) > 0$. This gives the range $X_{lim-} < X < X_{lim+}$, where X_{lim-} and X_{lim+} are the positive roots of the equation $X^3 + (J_m + 3)X + 2 = 0$. It can be proved that in this range of X, Eq. (20) always has a solution $\lambda_1 = \lambda_1(X, C_2)$ for any real value of C_2. Thus, this stretch range X is the region of the material model's validity and, accordingly, the region of definition of the phase plane. For $J_m = 97.3$, we have $X_{lim-} = 0.01994$ and $X_{lim+} = 10.0050$.

4.3. Phase plane and solitary wave solutions in the case of a quiescent fluid

Let us first consider a phase plane with $v_{f0} = 0$ and far-field stretches $\lambda_{10} = 1$ and $\lambda_{20} = 1.5$ (an axially unstretched but inflated state), which, according to Eq. (26), correspond to $p_0 \approx 0.808$. In this case, there are three stationary points: $X_s = 1.5$, 1.85, and 7.35 (Fig. 4a). The first point is of the saddle type (corresponding to a homogeneous far-field state), the second point is of the centre type, and the third point is of the saddle type. The vector field corresponding to the phase plane is shown in Fig. 5. Hereunder, we use the following notation of stationary points: the first letter is the type of point (c is the centre, and s is the saddle), and the second digit is the number of the stationary point; the far-field state

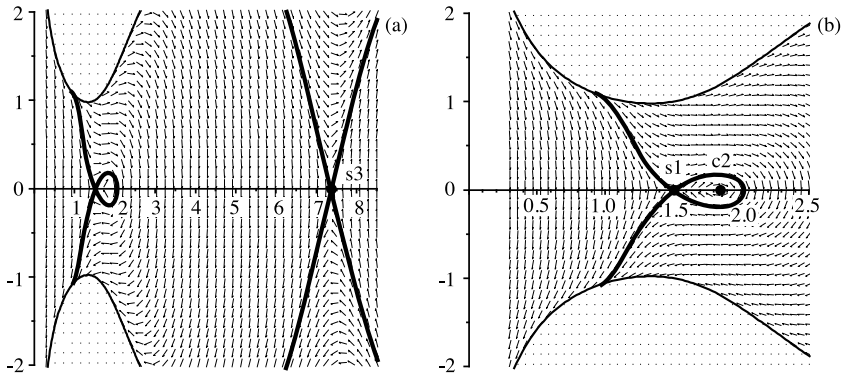

Fig. 5. Vector field of system (24) and separatrices of the stationary saddle points at $\lambda_{10} = 1$ and $\lambda_{20} = 1.5$. General view (a), enlarged view in the area of the separatrix loop (b).

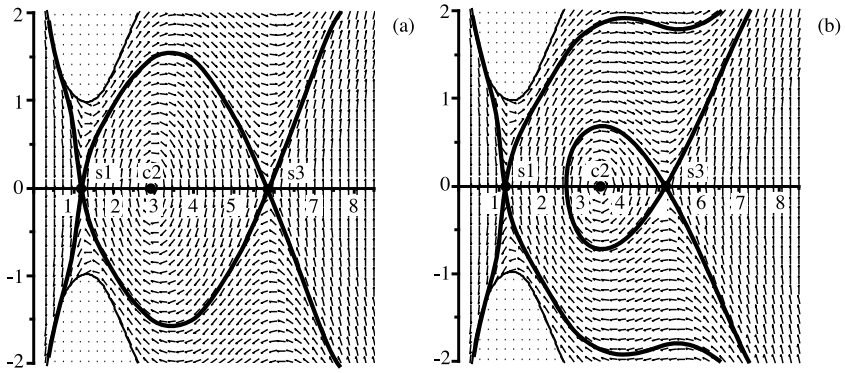

Fig. 6. Vector field of system (24) and separatrices of the stationary saddle points for $\lambda_{10} = 1$ and $\lambda_{20} = 1.1763$ (a), $\lambda_{20} = 1.15$ (b).

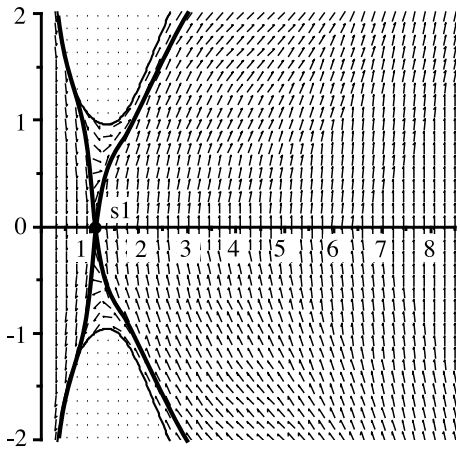

Fig. 7. Vector field of system (24) and separatrices of the stationary saddle point for $\lambda_{10} = 1$ and $\lambda_{20} = 1.11$.

always corresponds to number 1. As can be seen, there exists a solitary wave solution: the separatrix of the saddle s1, enveloping the centre c2 and returning to the original saddle. The solutions inside the saddle separatrix loop correspond to periodic tube swellings; any solution outside the separatrix loop tends to $X \to 0$ and $Y \to -\infty$ and approaches the limit line; i.e. such solutions exist only for a finite tube length. The separatrices of the saddle s3 are not closed: the separatrices going to the left cross the limit line; the separatrices going to the right reach the value X_{lim+}, at which the material reaches its stretch limit. Thus, with the parameters considered, there exists, in addition to the uniform state, the only standing solitary wave in the form of a localised tube swelling.

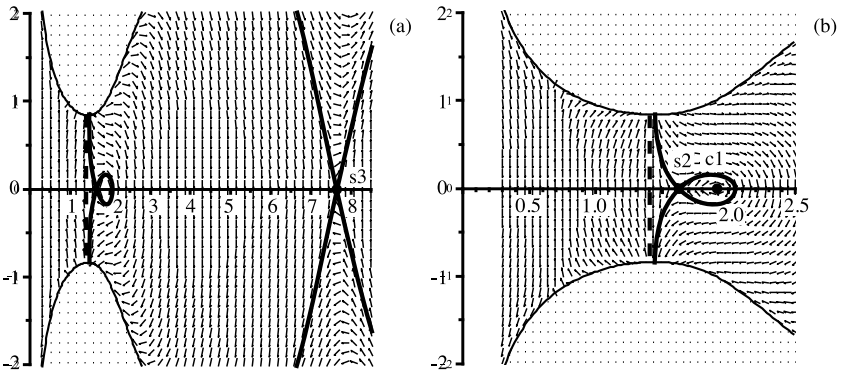

Fig. 8. Vector field of system (24) and separatrices of the stationary saddle points for $\lambda_{10} = 1$ and $\lambda_{20} = 1.9$. General view (a), enlarged view in the area of the separatrix loop (b). The vertical dashed line is the singularity of the vector field $W_1(X) = 0$.

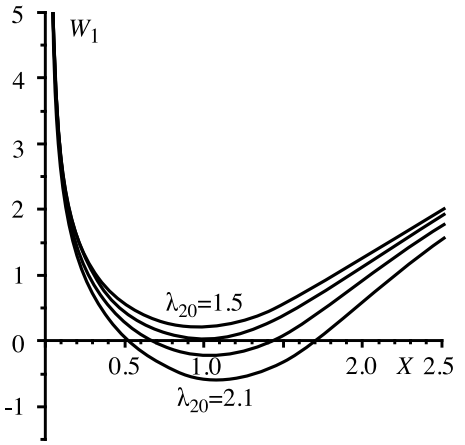

Fig. 9. Plot $W_1(\lambda_1(X), X)$ for $\lambda_{20} = 1.5,\ 1.7,\ 1.9,\ 2.1$.

Reducing stretch λ_{20} causes the centre c2 and saddle s3 to come closer together (Fig. 4a). The solitary wave solution disappears at $\lambda_{20} \approx 1.1763$, when the separatrix of the first saddle s1 becomes the separatrix of the saddle s3 (Fig. 6a), and the solitary wave transforms into a kink. With a further decrease in λ_{20}, the initial swelling solitary wave disappears, but a standing necking solitary wave (corresponding to a much more inflated far-field state) appears, in which the left separatrix of the saddle s3 goes around the centre c2 (Fig. 6b). For $\lambda_{20} \approx 1.14$, the saddle s3 and the centre merge (Fig. 4a), and the amplitude of the necking solitary wave tends to zero, after which there remains the only stationary point, the saddle s1, corresponding to the original far-field state. Obviously, for lower values of λ_{20} solitary wave solutions do not exist (Fig. 7).

Let us now consider a change in the phase plane with an increased λ_{20} from 1.5 and higher. The saddle point s1, corresponding to the uniform state, moves to the right, and the centre c2 moves to the left; for $\lambda_{20} = 1.69$, they pass through each other (Fig. 4b). For $\lambda_{20} > 1.69$, the type of stationary points changes: the saddle point s1 becomes the centre c1, and the centre c2 becomes the saddle s2. In this case, the solitary wave solution now corresponds to a less inflated far-field tube state (Fig. 8), while for the original far-field state, there remains only the uniform-tube solution. The parameter range in which there exists a family of standing swelling solitary waves for a quiescent fluid was first obtained by Pearce and Fu (2010).

Another bifurcation of the phase plane occurs at $\lambda_{20} = 1.73$. In this case, a range of X appears for which $W_1(\lambda_1(X), X) < 0$ (Fig. 9); i.e. the region in which the axial stress becomes compressive. In this range, the vector field (24) turns around, and at the points at which $W_1 = 0$, it has a singularity (note that $W_{11}(\lambda_1(X), X)$ is always positive; i.e. there are only singularities associated with zero longitudinal stress). Thus, solutions starting in the region $W_1 > 0$ cannot penetrate the area left of the line $W_1 = 0$ but end on the limit line (Fig. 8). With a further increase in λ_{20}, the range in which $W_1 < 0$ expands and captures the saddle s2, which then again becomes the centre c2 (Fig. 10). There are no standing solitary wave solutions.

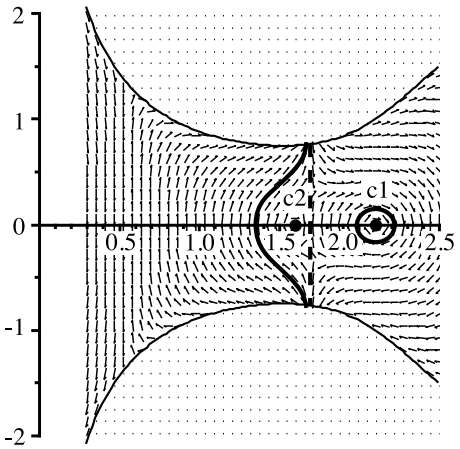

Fig. 10. Vector field of system (24) and integral trajectories enveloping the centres for $\lambda_{10} = 1$ and $\lambda_{20} = 2.1$. The vertical dashed line is the singularity of the vector field $W_1(X) = 0$.

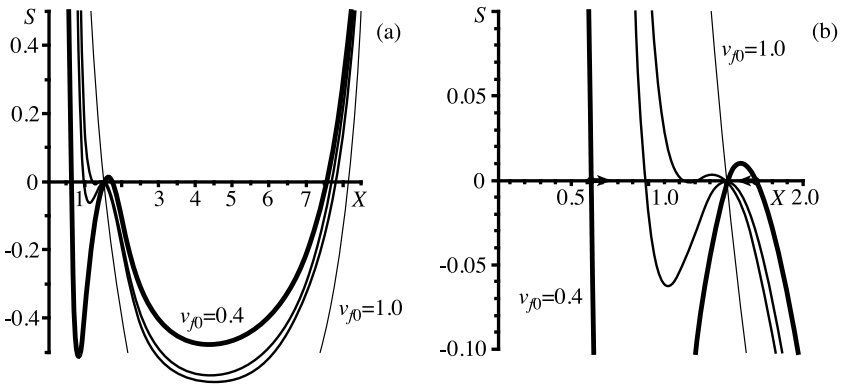

Fig. 11. Plot of the function $S(X)$ at $\lambda_{10} = 1$, $\lambda_{20} = 1.5$, and $v_{f0} = 0.4$, 0.58, 0.64, 1.0 (a), enlarged view in the region of small X (b). The arrows show the direction of movement of the roots with increasing v_{f0}.

4.4. Phase plane and solitary waves in the case of a moving fluid

To be specific, we put $n = 0$ (a uniform fluid velocity distribution); as noted above, other values of n yield rescaling of v_{f0}, but the qualitative picture will obviously remain the same. With far-field parameters $\lambda_{10} = 1$, $\lambda_{20} = 1.5$, and $v_{f0} < 0.0624$, the structure of the phase plane is the same as for a quiescent fluid. For $v_{f0} \geq 0.0624$, in addition to the three stationary points, two more points appear in the vicinity of $X = 0.038$: the centre c4 and the saddle s5. As the fluid velocity increases, the saddle moves to the left and, for $v_{f0} > 0.37$, leaves the phase plane through the left boundary; we will not consider it further. The centre moves to the right (Fig. 11) and is located to the left of the saddle s1, which corresponds to the far-field state. Due to the presence of a centre, the vector field turns around for small X (Fig. 12): if for $v_{f0} = 0$ it was directed downwards, now it is directed upwards, and there are closed trajectories enveloping a new stationary centre.

There are two standing solitary waves simultaneously emerging from the saddle s1 corresponding to the uniform state: the localised swelling in which the separatrix loop envelops the right centre c2 and the localised necking in which it envelops the left centre c4 (Fig. 12). Both solutions are shown in Fig. 13 as functions $\lambda_2(x)$.

An increase in the flow velocity v_{f0} leads to changes in the phase plane, as with an increase in λ_{20} for the quiescent fluid. Namely, the right centre c2 moves to the left, and at $v_{f0} \approx 0.58$, it merges and passes through the saddle s1, which corresponds to a homogeneous state (Fig. 11). Then the types of both stationary points are reversed. The swelling and necking solitary waves still exist, but their conditions at infinity correspond to a smaller λ_{20} than in the original far-field state (Fig. 14a).

At $v_{f0} \approx 0.64$, the two left stationary points, the saddle s2 and the centre c4, approach, merge, and disappear (Fig. 11). For larger values of the velocity, two stationary points remain: the centre c1, which corresponds to the far-field state (Fig. 14b), and the saddle s3, which corresponds to much larger stretches; no standing solitary wave solutions exist. With

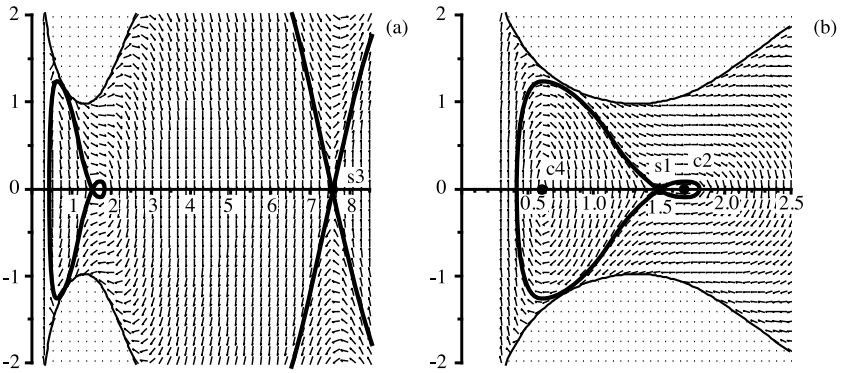

Fig. 12. Vector field of system (24) and separatrices of the stationary saddle points for $\lambda_{10} = 1$, $\lambda_{20} = 1.5$, and $v_{f0} = 0.4$. General view (a), enlarged view in the area of the separatrix loops (b).

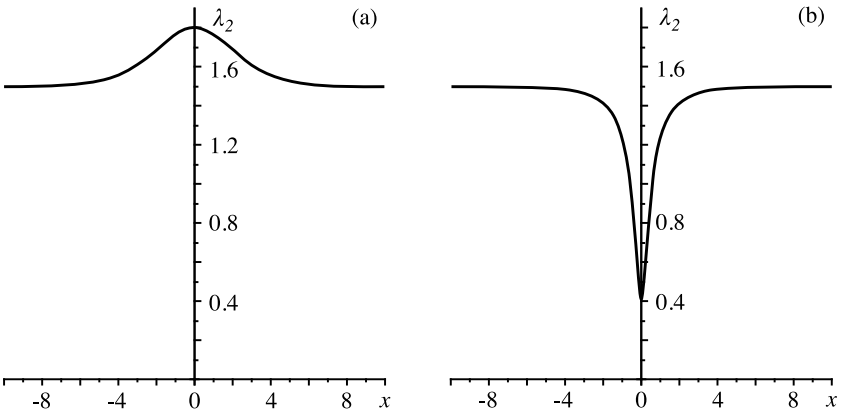

Fig. 13. Swelling (a) and necking (b) solitary waves $\lambda_2(x)$ for $\lambda_{10} = 1$, $\lambda_{20} = 1.5$, and $v_{f0} = 0.4$.

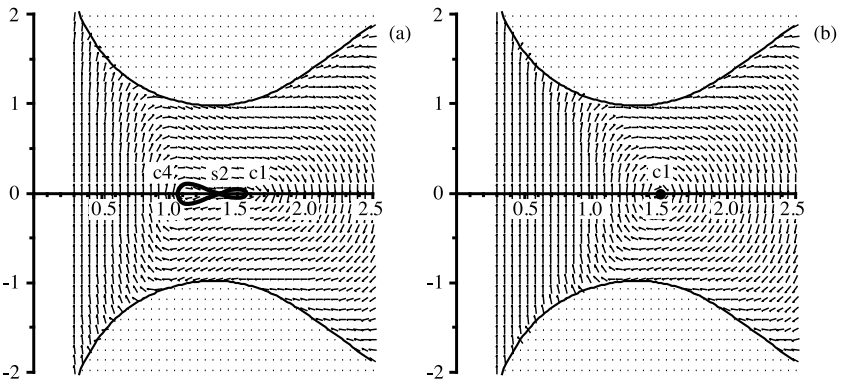

Fig. 14. Vector field of system (24) and separatrices of the stationary saddle points for $\lambda_{10} = 1$, $\lambda_{20} = 1.5$, and $v_{f0} = 0.63$ (a), $v_{f0} = 1.0$ (b).

an increase in speed, the saddle s3 gradually moves to the right, and for $v_{f0} > 9$, it leaves the phase plane through its right boundary. At higher speeds, the only stationary point remains, the centre c1.

5. Steady states in the case of a viscous fluid

As can be seen from system (23), for $\tau \neq 0$ the vector field becomes non-symmetric with respect to the X axis due to the term $-\tau XY/W_{11}$. For the Gent model $W_{11} > 0$; therefore, each centre point becomes a stable focus; each saddle point remains a saddle, but its separatrices rotate somewhat clockwise. In addition, the values of p_0 and C_2, which were associated with the tube state at infinity for an inviscid fluid, become non-constant in the viscous case: $p_0(x)$ is

a decreasing function, $C_2(x)$ is a growing function, and therefore $\lambda_1 = \lambda_1(X, x)$. Note that the functions $p_0(x)$ and $C_2(x)$ themselves depend on the solution; i.e. system (23), strictly speaking, is not a system of differential equations. Parameters λ_{20} and v_{f0}, which also corresponded to the tube state at infinity for the case of an inviscid fluid, can now refer to any tube cross-section. The stationary points of the phase plane, i.e. the solutions of Eq. (25), now also depend on x. The motion of the integral curve can be represented as the motion along the vector field, which itself changes with x; moreover, for each solution the vector field changes in its own way.

5.1. Stretch limit states as $x \to \pm\infty$

First, consider possible deformed steady states, i.e. λ_1 and λ_2 independent from x as $x \to \pm\infty$. In this case, we have

$$p_0(x) = -2\tau\frac{\lambda_1}{\lambda_2}x = -Px, \quad P = 2\tau\frac{\lambda_1}{\lambda_2} > 0 \qquad C_2(x) = \tau\lambda_1^2\lambda_2 x.$$

The constants in $p_0(x)$ and $C_2(x)$ for large values of $|x|$ can be neglected.

Consider the solution of Eq. (20) for the Gent material model (Section 4.2):

$$W - \lambda_1 W_1 = \frac{1}{2}GJ_m \ln a - Ga\left(\lambda_1^2 - (\lambda_1\lambda_2)^{-2}\right) = C_2(x) = \tau\lambda_1^2\lambda_2 x.$$

Obviously, this equation can be satisfied as $x \to \pm\infty$ only if $a(x) \sim Ax \to \infty$ with $A = \text{const}$, i.e.

$$a^{-1} = 1 - \frac{\lambda_1^2 + \lambda_2^2 + (\lambda_1\lambda_2)^{-2} - 3}{J_m} \to 0. \tag{27}$$

Neglecting the first term ($\ln a \ll a$), we obtain

$$A = -\frac{\tau}{G}\lambda_1^2\lambda_2\left(\lambda_1^2 - (\lambda_1\lambda_2)^{-2}\right)^{-1}.$$

Since $a > 0$, it is also necessary that the following inequalities are satisfied:

$$\lambda_1^2 - (\lambda_1\lambda_2)^{-2} < 0, \quad x \to +\infty; \qquad \lambda_1^2 - (\lambda_1\lambda_2)^{-2} > 0, \quad x \to -\infty. \tag{28}$$

Expression (27) gives the relationship between the possible limit values of λ_1 and λ_2. The limit value of W_2 has the form

$$W_2 = Ga\left(\lambda_2^2 - (\lambda_1\lambda_2)^{-2}\right)\lambda_2^{-1} = Bx, \quad B = -\tau\lambda_1^2\frac{\lambda_2^2 - (\lambda_1\lambda_2)^{-2}}{\lambda_1^2 - (\lambda_1\lambda_2)^{-2}}.$$

Next, consider equation (25) as $x \to \pm\infty$. Leaving only the leading terms, we have

$$-P\lambda_2 x - \frac{Bx}{\lambda_1} = 0 \quad \Rightarrow \quad 2 = \frac{\lambda_2^2 - (\lambda_1\lambda_2)^{-2}}{\lambda_1^2 - (\lambda_1\lambda_2)^{-2}}. \tag{29}$$

Let us prove that there always exist unique limit states satisfying equations (27) and (29) and inequalities (28). Rewrite them, denoting $\lambda_1^2 = l_1$ and $\lambda_2^2 = l_2$:

$$l_1^2 l_2 + l_1 l_2^2 - (3 + J_m) l_1 l_2 + 1 = 0, \tag{30}$$

$$2(1 - l_1^2 l_2) = 1 - l_1 l_2^2, \tag{31}$$

$$1 - l_1 l_2^2 > 0, \quad x \to +\infty; \qquad 1 - l_1 l_2^2 < 0, \quad x \to -\infty. \tag{32}$$

Eqs. (30) and (31) are equivalent to the system

$$l_1 l_2(l_1 + l_2 - (3 + J_m)) = -1 = l_1 l_2(l_2 - 2l_1).$$

From here we obtain

$$l_1 = \frac{3 + J_m}{3}, \quad l_2 = l_1 \pm \sqrt{l_1^2 - \frac{1}{l_1}}.$$

As $l_1 > 1$, the value of l_2 is always real and positive.

It is easy to verify that the 'plus' sign before the root satisfies inequality (32) as $x \to -\infty$ and the 'minus' sign as $x \to +\infty$. As $x \to -\infty$, the tube is swollen and axially stretched ($\lambda_1 > 1$, $\lambda_2 > 1$): far upstream, the stretched state tends to the limit state, and the tensile stresses tend to infinity. In this case, the axial stress in the tube wall σ_1 is balanced by the fluid viscous force, which axially stretches the tube sections lying upstream, and the circumferential stress σ_2 is balanced by pressure, which grows unlimitedly upstream. As $x \to +\infty$, the tube is also axially stretched but compressed in the circumferential direction ($\lambda_1 > 1$, $\lambda_2 < 1$). In this case, both axial and circumferential stresses are compressive and tend to infinity. The axial stress σ_1 downstream is balanced by the viscous force, which compresses the tube axially, and the circumferential stress σ_2 is balanced by pressure, which decreases unlimitedly due to viscous losses. We note

that the limit states do not depend neither on the fluid properties nor on the values of the constants but depend only on parameter J_m of the tube material.

By direct calculation, taking into account equation (29) and a large value of a, it can be proved that for both limit states $dS/dX > 0$, which means that the limit stationary point of a 'frozen' vector field at large $|x|$ is saddle point as $x \to -\infty$ and stable focus point as $x \to +\infty$.

For $J_m = 97.3$, which corresponds to rubber, we have limit axial stretch $\lambda_1 = 5.782156$, and limit circumferential stretches $\lambda_2 = 0.021149$ as $x \to +\infty$ and $\lambda_2 = 8.177176$ as $x \to -\infty$.

5.2. Evolution of the tube when moving from infinity

Let us now investigate the possibility of combining limit states as $x \to -\infty$ and $x \to +\infty$ by a single integral curve, i.e. constructing a steady solution for the entire infinitely long tube conveying a viscous fluid. To do this, we divide the tube into three sections. Two sections are neighbourhoods of infinities as $x \to -\infty$ and $x \to +\infty$, where the limit stationary points continuously move when x changes, but they remain the only stationary points of the phase plane (or, if other stationary points appear, they do not interact with the limit stationary point). The third section is the central section, where new stationary points appear and can interact with stationary points that came from neighbourhoods of infinity. In a certain cross-section of the central segment, we put the origin of the x axis, and specify stretches $\lambda_1 = \lambda_{10}$ and $\lambda_2 = \lambda_0$ and fluid velocity $v_f 0$. We do not specify pressure in this cross-section; below we will show that there is only one pressure value that provides the existence of a solution for $-\infty < x < \infty$. In this section, we study the behaviour of integral trajectories with a motion of limit stationary points.

5.2.1. Evolution of the tube as $x \to -\infty$

First, consider the limit saddle point as $x \to -\infty$. As the absolute value of x decreases, the value of X_s corresponding to this stationary point decreases; in the central part of the tube, this saddle continuously passes to the left saddle s3 in Fig. 5. It is easy to see from the local structure of the vector field in the vicinity of the moving saddle that there always exists an integral curve, which for each x is located near the moving saddle point and does not 'fall' onto the separatrix leaving it. Moreover, for $x \to -\infty$, such an integral curve tends to the limit position of the saddle (a limit state of the tube). Thus, the moving saddle 'leads' such an integral curve. When the saddle moves to the left, the integral curve follows below it; the lower the curve the higher the speed of the saddle. When the saddle moves to the right, the integral trajectory, on the contrary, follows the saddle above it.

The existence of an integral trajectory following the moving saddle can also be seen from the explicit solution of the model problem

$$X'' + 2cX' = A(X - X_0(x)), \quad A > 0, \quad c > 0,$$

where $X_0(x)$ is the variable position of the saddle and $X(x)$ is an unknown function. The solution of this equation has the form

$$\begin{aligned} X(x) &= X_0(x) + \\ &+ e^{-cx}\left(\frac{1}{2\sqrt{\varkappa}}\left(\int_{x_0}^{x} e^{-\sqrt{\varkappa}\xi}\beta(\xi)d\xi\, e^{\sqrt{\varkappa}x} - \int_{x_0}^{x} e^{\sqrt{\varkappa}\xi}\beta(\xi)d\xi\, e^{-\sqrt{\varkappa}x}\right) + c_1 e^{\sqrt{\varkappa}x} + c_2 e^{-\sqrt{\varkappa}x}\right), \\ \varkappa &= A + c^2, \qquad \beta(x) = (-X_0'' - 2cX_0')e^{cx}. \end{aligned}$$

It is easy to see that if the saddle position has moved along a finite segment x from one fixed position to another (in this case, $\beta(x) \neq 0$ only on a finite segment x, and the integrals tend to constants as $x \to +\infty$), then there exists a solution that asymptotically tends to the initial state as $x \to -\infty$ and to the final state as $x \to +\infty$.

Thus, before reaching the central section of the tube, where the interaction of the stationary points occurs, there exists an integral trajectory coming from $-\infty$ following the saddle.

5.2.2. Evolution of the tube as $x \to +\infty$

Now consider the integral trajectory following from $x \to +\infty$ to the central section. It will be shown below that it is necessary that in the central part of the tube the stationary point continuously passes to the right saddle s1 in Fig. 5. For such a continuous evolution, it is necessary that during the motion from $x \to +\infty$, no new stationary point emerges. If such a point arises (it must be a focus that in the inviscid case corresponds to the centre c4 in Fig. 12), it will separate two stationary points: the analogues of the right saddle s1 in Fig. 12 and the saddle point s5 lying near the left boundary of the phase plane and corresponding to the limit state at $x \to +\infty$. A continuous transition of one stationary point to another with a change in x takes place only for sufficiently small v_{f0}, for which there is no 'intermediate' stationary point. In particular, the calculation shows that for $\lambda_1(0) = \lambda_{10} = 1$, $\lambda_2(0) = \lambda_{20} = 1.5$, and the initial condition $p_0(0)$ defined by the equilibrium condition in inviscid flow (26), the transition to $x \to +\infty$ occurs without the formation of an intermediate stationary point for $v_{f0} \leq 0.0635$, which is close to the value at which the intermediate stationary point is absent for $x = 0$ (Section 4.4).

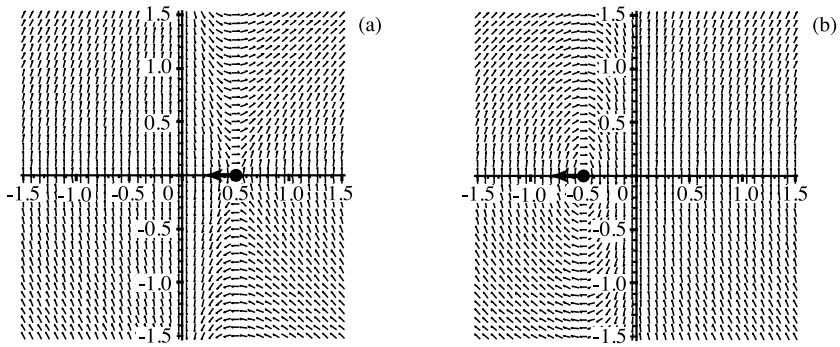

Fig. 15. Phase plane of the 'frozen' equation (33) for $x = -0.5$ (a) and $x = 0.5$ (b). The arrow shows the direction of the stationary point's motion with increasing x.

Below, we will assume that this condition is satisfied; otherwise, as will be shown below, it is impossible to connect the limit states of the tube as $x \to \pm\infty$.

The limit stationary point for $x \to +\infty$ is a stable focus. It is easy to see from the structure of the vector field that when the focus moves, there is a trajectory that remains in its vicinity and rotates around it; when the focus movement stops, the trajectory asymptotically tends to it. As a result, as in the case of a saddle at $x \to -\infty$, there is an integral trajectory 'following' the focus motion.

The existence of such a trajectory is also evident from the explicit solution of the model problem

$$X'' + 2cX' = -B(X - X_0(x)), \quad B > 0, \quad c > 0,$$

where $X_0(x)$ is the variable focus position and $X(x)$ is an unknown function. The solution of this equation has the form

$$\begin{aligned} X(x) &= X_0(x) + \\ &+ \frac{e^{-cx}}{\sqrt{\delta}} \left(\int \cos(\sqrt{\delta}\xi)\beta(\xi)d\xi \sin(\sqrt{\delta}x) - \int \sin(\sqrt{\delta}\xi)\beta(\xi)d\xi \cos(\sqrt{\delta}x) \right) + \\ &+ c_1 \cos(\sqrt{\delta}x)e^{-cx} + c_2 \sin(\sqrt{\delta}x)e^{-cx}, \qquad \delta = B - c^2. \end{aligned}$$

It is seen that if the location of the focus tends to a constant as $x \to \infty$, then all the trajectories, including those coming out of the vicinity of its initial position, asymptotically approach its final position.

Hereunder we will assume that the central section of the tube, where we must connect the trajectory coming out from $x \to -\infty$ and going to $x \to +\infty$, is inflated: for the inviscid case, there are several stationary points, and there exist standing solitary waves. Then the axial stress in the central section is tensile so that $W_1 > 0$. However, it was shown above that as $x \to +\infty$, the axial stress is compressive, i.e. $W_1 < 0$, which means that there is a point X_c at which $W_1 = 0$; along the vertical line $X = X_c$ the vector field (23) has a singularity. In addition, when passing through a singularity, the type of the stationary point changes: a saddle becomes a focus and vice versa. Only one integral trajectory passes through the singularity line; all other trajectories end at the limit line $Y = \lambda_1(X, x)$. Namely, when a stationary point passes through a line of zero axial stress below the stationary point, the vectors are horizontal. If we follow the vector field at a distance from the stationary point at which the length of the horizontal vector is equal to the stationary point's speed, a smooth passage through the singularity is ensured; all other integral trajectories turn up or down before the singularity and end at the limit line.

The following model equation is an illustration of the transition through a singularity:

$$X'' = A\frac{X + x}{X}. \tag{33}$$

The equation's stationary point is a saddle for $x < 0$ and a centre for $x > 0$. The vector fields for $x = -0.5$ and $x = 0.5$ are shown in Fig. 15. Its exact solution $X(x) = -x$ for each x corresponds to a stationary point; on the phase plane, due to the motion of the stationary point, the integral trajectory moves under it along the line $Y = -1$. Any other solution, starting from $x < 0$, cannot penetrate the line $X = 0$ and remains to its right, turning up or down before this line.

It is important that this unique trajectory corresponds to the transition to $x \to +\infty$ only when the point X_c at which the change in sign of W_1 takes place is unique. If there are more such points, then it is impossible to have a trajectory penetrating several singularities: the condition of passing through the first one selects a single integral curve that can no longer, except for special cases, pass through other singularities. Further, we will assume that point X_c is unique. For the parameters $\lambda_1(0) = \lambda_{10} = 1$ and $\lambda_2(0) = \lambda_{20} = 1.5$ and the initial condition $p_0(0)$ determined from Eq. (26), the transition to $x \to +\infty$ occurs with a single X_c for $v_{f0} \leq 0.0565$. In particular, this condition is satisfied in the example constructed below in Section 5.4.

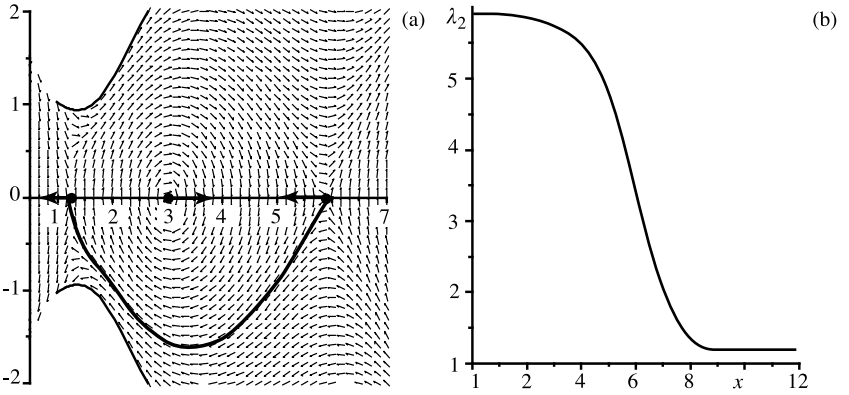

Fig. 16. Transition in the central part of the tube from the vicinity of the stationary point as $x \to -\infty$ to the neighbourhood of the stationary point as $x \to +\infty$ for the initial ($x = 0$) parameters $\lambda_{10} = 1$, $\lambda_{20} = 1.5$, $v_{f0} = 0.05$, and $p_0 \approx 0.484$. The integral curve in the phase plane (the vector field corresponds to the state at $x = 0$, the arrows show the direction of motion of the stationary points with increasing x) (a); plot $\lambda_2(x)$ (b).

Note that for fluid velocities exceeding the critical values (at which either an intermediate stationary point or more than one X_c appear) and for realistic values of fluid viscosity, the inability to continue the trajectory as $x \to +\infty$ arises at sufficiently large values of x, exceeding hundreds or thousands of tube radii. As a result, although it is mathematically impossible to continue the solution to infinity, the region of its existence exceeds any lengths of tubes conveying fluid that are encountered in applications.

5.3. Connection of integral trajectories from infinities in the central part of the tube

Thus, from both left and right infinities, at a sufficiently low speed v_{f0}, it is possible to continue an integral trajectory to the central region of the tube, where both stationary points are saddles. Expecting solutions with a solitary wave form, we will assume that in the central part, the structure of the 'frozen' phase plane qualitatively corresponds to Fig. 5 (except that the centre c2 becomes a stable focus). When increasing x (moving downstream), the focus and the right saddle merge and disappear; when decreasing x (moving upstream), the focus and the left saddle merge and disappear; in both cases, there is a homoclinic bifurcation of the vector field. The remaining saddle evolves into a limit state, as shown in the previous section.

For such a configuration, in which at a certain x a stable focus exists between the two saddles, it is impossible to transform the limit saddles into each other with a change in x. However, under certain conditions, there is an integral trajectory connecting the saddles and bypassing the focus from below. More precisely, from the vicinity of the right saddle with increasing x, the integral trajectory comes into the vicinity of the left saddle. For this, it is necessary that the focus is located between the saddles in such a way that the integral trajectory from the neighbourhood of one stationary point comes into the neighbourhood of the other (Fig. 16). To realise such a configuration, there are two free parameters in the problem, since the pressure p_0 and C_2 are defined to within a constant. In the absence of viscosity, these constants are determined by the parameters at infinity, but in the presence of viscosity, these constants can be chosen arbitrarily, since both pressure and C_2 tend to infinity at $x \to \infty$. Only one of these parameters is essentially arbitrary, since their simultaneous change in a certain combination corresponds only to a shift in the origin of the x axis (or, equivalently, a shift of the entire tube to the left or to the right). Thus, due to this one free parameter, e.g. pressure, it is possible to locate the focus so that the integral trajectories for $x \to -\infty$ and $x \to +\infty$ are connected in the central part of the tube with a focus bypass from below.

Small changes in pressure will lead to small changes in the integral trajectory, up to the moment of intersection with the singularity (the line of change in the sign of W_1, i.e. a change of tensile longitudinal stress to compressive stress). As shown in Section 5.2.2, there is only one trajectory that penetrates this singularity, while the other trajectories on the phase plane turn up or down and end at the limit line. Thus, the parameter (e.g. pressure) has the only value at which the integral trajectory passes through the singularity. After that, the trajectory moves in an uncontrolled way. However, since it moves in the vicinity of a stable focus (which moves to the left with increasing x), it does not leave its vicinity and asymptotically tends to the limit state as $x \to +\infty$.

Now we can explain why it is necessary that during the evolution of a stationary point as $x \to +\infty$, an intermediate stationary point should not occur (Section 5.2.2). As in the central tube section, at a certain position of the three stationary points, it would be possible to connect the two outer points by passing the middle point from below (unlike in the central part, here the saddles and focuses are switched if the interaction occurs at $W_1 < 0$; however, this does not preclude the possibility of their connection by an integral trajectory). To do this, the middle stationary point must be located between the outer points in such a position that the trajectory from the neighbourhood of the right point comes into the

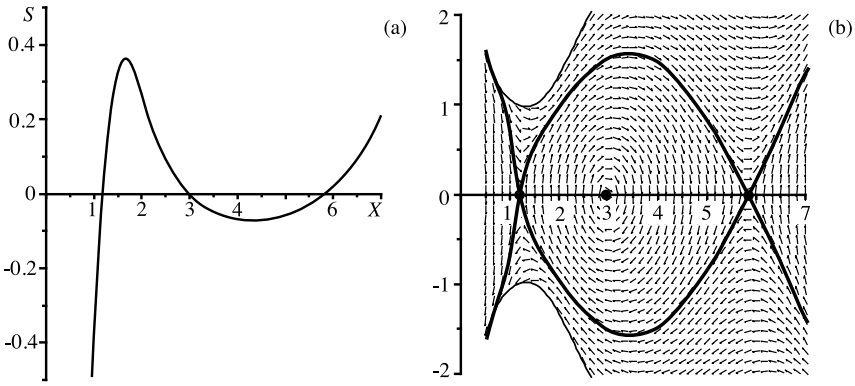

Fig. 17. Plot $S(X)$ (a) and phase plane and integral curve in the absence of viscosity (b) for the parameters $\lambda_1(0) = \lambda_{10} = 1$, $\lambda_2(0) = \lambda_{20} = 1.5$, $v_{f0} = 0.05$, and $p_0 \approx 0.477$.

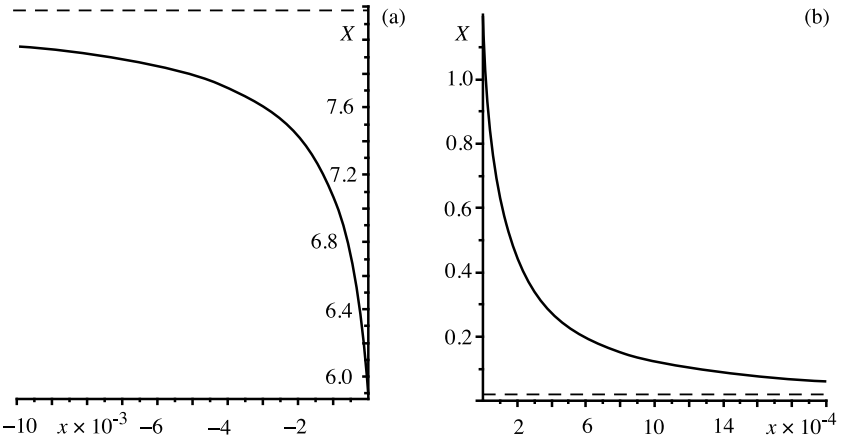

Fig. 18. The calculated evolution of the position of the stationary point to infinity for $x < 0$ (a) and for $x > 12$ (b) for the initial ($x = 0$) parameters $\lambda_{10} = 1$, $\lambda_{20} = 1.5$, $v_{f0} = 0.05$, and $p_0 \approx 0.484$. The dashed lines are the limit values.

neighbourhood of the left point. However, we do not have other free parameters to organise such a connection. Therefore, the only way to continue the trajectory to $x \to +\infty$ is to prevent the occurrence of the focus, which is ensured by the requirement that the fluid velocity in the central tube segment is sufficiently small: $v_{f0} < v_{f0\mathrm{cr}}$. The only special case may be a fluid velocity $v_{f0} > v_{f0\mathrm{cr}}$ such that the desired location of the stationary points occurs simultaneously with penetration of the singularity; however, this exceptional case is not of general interest, since it cannot be realised in reality: an arbitrarily small deviation from this value v_{f0} will lead to the end of the trajectory at the limit line and the tube's collapse.

5.4. An example of a solution for an infinitely long tube

Consider an example of a solution for an infinitely long tube. The calculations were performed numerically, separately for the central tube section and the neighbourhoods of infinity. In the central region, the full differential equation (19) was solved by the Euler method taking into account the algebraic relation (20). The calculation took into account the change in $p_0(x)$ and $C_2(x)$ according to formulas (14) and (18) (in dimensionless form). The values of the integrals were updated at each x-step by the rectangle method simultaneously with the numerical integration of Eq. (19).

In the vicinity of infinities, the numerical integration of the full problem is practically impossible, because the integral trajectories tend to 'fall' onto the separatrices coming out of the saddles and, therefore, are extremely sensitive to the initial conditions. For example, to keep the trajectory near a stationary point at a distance of ~ 1 tube radius, an accuracy of setting the initial conditions of $\sim 10^{-6}$ is required; and the required accuracy increases exponentially with increasing tube length. Thus, although a solution remaining in the vicinity of the saddle exists, it is almost impossible to obtain it numerically on a long x-interval. To calculate the evolution of the position of the stationary points, it was assumed that their motion is rather slow and that the derivative λ_2' in Eq. (19) can be neglected. Then, replacing it by zero, this equation becomes algebraic; it was solved numerically for given values of $p_0(x)$ and $C_2(x)$. A segment of the x axis of a sufficiently

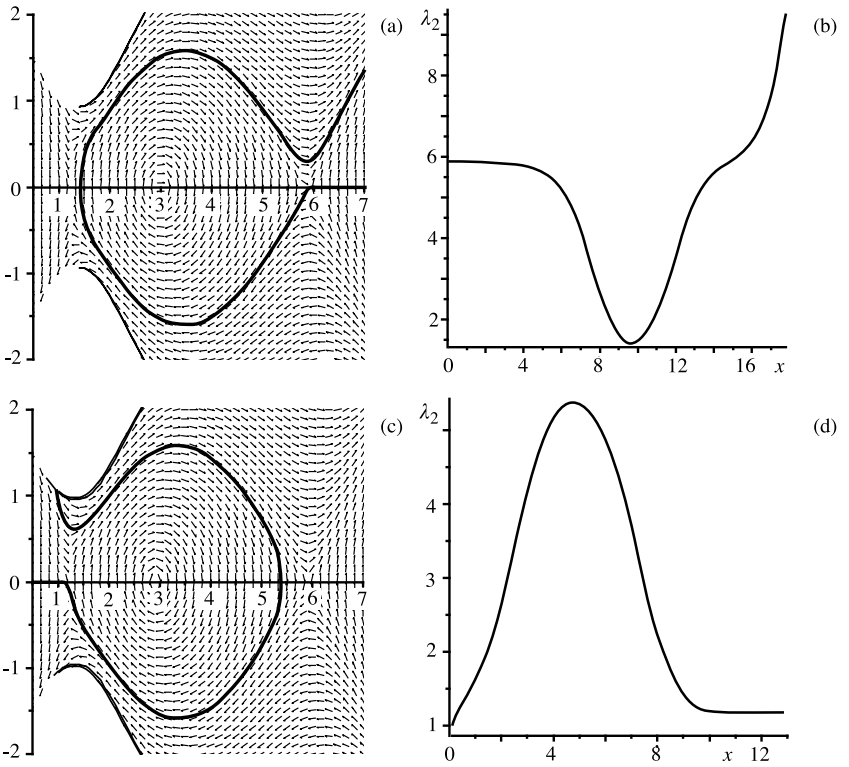

Fig. 19. Solitary-wave-like solutions for an infinitely long tube as $x \to -\infty$ (a, b) and for an infinitely long tube as $x \to +\infty$ (c, d). The integral trajectory on the phase plane (the vector field corresponds to $x = 0$) (a, c), and the solution $\lambda_2(x)$ (b, d) are shown.

large length (directed either to $+\infty$ or $-\infty$) was divided into a sufficiently fine grid, along which the integrals $p_0(x)$ and $C_2(x)$ and, accordingly, the position of the stationary point $\lambda_2(x)$ changed. Although this approach is approximate, it yields a rather accurate calculation of the stationary points' motion, because outside the central section they move slowly; for $x \to \pm\infty$ their positions tend to fixed values, while the speed of motion $\lambda_2'(x)$ tends to zero.

In the calculations, for simplicity, the power-law index $n = 0$ was taken; however, it is clear that for any other value, the solution will be qualitatively the same. Since the fluid friction in this case is constant, formula (21) can be rewritten as follows: $\tau = 8v_{f0}^2/\mathrm{Re}_0$, where the index '0' corresponds to an initial section of the tube. In the calculations, the initial Reynolds–Metzner–Read number $\mathrm{Re}_0 = 100$ was set.

We set the parameters $\lambda_1(0) = \lambda_{10} = 1$, $\lambda_2(0) = \lambda_{20} = 1.5$, and $v_{f0} = 0.05$ and selected a pressure $p_0 = 0.477$ so that the focus of the 'frozen' vector field is located between two saddles, which have common separatrices (Fig. 17). We take this position for $x = 0$ and consider this value to be the left border of the central tube section. However, due to viscosity, the vector field shown in Fig. 17 will evolve: the right saddle and centre approach each other, while the left saddle moves to the left. Therefore, taking into account viscosity, the integral trajectory at this initial value p_0 will come to the right of the neighbourhood of the left saddle, and a pressure correction is necessary. Calculations show that for $p_0 \approx 0.484$, the trajectory, taking into account viscosity, comes into the vicinity of the left saddle (Fig. 16). Thus, this and very similar initial pressure values provide the connection of the neighbourhoods of the stationary points that come from infinity by a single integral curve.

The numerically calculated motion of the stationary points when moving to infinity for $x < 0$ and $x > 12$ is shown in Fig. 18. As can be seen, they are continuously moving to their asymptotic values. Note that at $x \approx 580$, the value of $W_1(x)$ becomes negative and then retains its sign for an unlimited increase in x; at the change in sign, the stationary point's location is $X \approx 1.13$. Since after changing the sign, the saddle becomes a stable focus, the monotonic decrease in $X(x)$ is replaced by an oscillatory motion.

In dimensional terms, taking a ratio $h/R = 0.1$, the shear modulus of rubber $G = 10^6$ Pa, and a fluid density $\rho_f = 1000$ kg/m^3, the constructed solution corresponds to a fluid velocity $v_{f0} = 0.5$ m/s and a pressure $p_0 = 48.4$ kPa. A Reynolds number $\mathrm{Re} = 100$ corresponds to a fluid friction $\tau = 20$ Pa.

5.5. Existence of solitary-wave-like solutions

The solution constructed above corresponds to a monotonic downstream change from the inflated limit state to the compressed limit state of the tube. Let us show that a solitary wave solution, i.e. a solution enveloping focus, does not

exist. It can be seen from the calculations that, with an increase in x in the central part of the tube, the focus moves to the right, and both saddles move to the left. Suppose that $p_0(0)$ is chosen so that the trajectory, starting from the vicinity of the right saddle point, just does not reach the left saddle point and makes one revolution around the focus point. However, due to the movement of the focus to the right, and the movement of the right saddle to the left, the position of the trajectory after the revolution will be above the right saddle. The trajectory will then follow the upper right separatrix to the boundary of the phase plane, where the tube will collapse.

Thus, solutions in the form of a standing solitary wave, i.e. with a single local swelling or necking of the tube, do not exist for an infinitely long tube. However, they exist for a semi-infinite tube. For a tube that is unbounded as $x \to -\infty$, an example is given in the previous paragraph; it is possible to select $p_0(0)$ and a final value $x > 0$ to make one revolution around the focus; as a result, we have a necking solitary wave. For a tube that is unbounded as $x \to +\infty$, we can choose $p_0(0)$ and start the path above the initial position of the upper right separatrix of the left saddle, after which it continues indefinitely as $x \to +\infty$. The result is a swelling solitary wave. Both examples of solitary waves at semi-infinite tubes are shown in Fig. 19.

Obviously, for a tube of finite length, there are solutions that monotonically connect two states and make a certain number of revolutions around the focus (but always a finite number because sooner or later the focus will disappear from the phase plane due to the influence of viscosity), each revolution corresponding to swelling or necking of the tube.

6. Conclusions

In this paper, we analysed the possible steady states of an elastic tube made of an incompressible hyperelastic Gent material (rubber), conveying a viscous fluid with power-law rheology. It is proved that for a quiescent fluid (or, equivalently, if a constant pressure is set in the tube) in a tube that is axially unstretched at infinity ($\lambda_{10} = 1$), a standing solitary wave in the form of a localised swelling exists for a range of far-field circumferential stretches $1.18 < \lambda_{20} < 1.69$. This result was previously obtained by Pearce and Fu (2010).

In the case of the motion of an inviscid fluid (generally, with a non-uniform cross-sectional velocity distribution) for $\lambda_{10} = 1$, $\lambda_{20} = 1.5$, and a dimensionless velocity $0.063 \leq v_{f0} \leq 0.58$, there exists, simultaneously with the standing swelling solitary wave, a standing necking solitary wave. At a lower fluid velocity, there is only a swelling solitary wave; for larger velocities, no solitary waves exist. Note that in a model of a geometrically and physically linear tube, in which only the nonlinearity of the flow was taken into account (Poroshina and Vedeneev, 2018), there always exists, for any nonzero flow velocity, only a standing necking solitary wave. Thus, both the existence of a standing swelling solitary wave and the limited range of fluid velocities for which a standing necking solitary wave exists are consequences of the physical and geometrical nonlinearities of the tube model.

When a viscous fluid moves, there are limit stretch states of the tube as $x \to -\infty$ and $x \to +\infty$, with the stretches λ_1 and λ_2 tending to constants but the stresses tending to infinities to compensate for the fluid pressure and the longitudinal stress caused by the fluid viscosity, which are infinitely growing upstream and infinitely decreasing downstream. The transition between these limit states occurs in the central section of the tube and exists only if the fluid velocity is sufficiently small. In this case, for given stretches λ_1 and λ_2 and flow speed v_f in a chosen cross-section, there is a unique solution linking the states at infinity in the form of a monotonic decrease in the radius downstream, i.e. a kink-like solution. Localised swelling or necking solutions for a tube that is infinitely long in both directions do not exist. However, such solutions exist if the tube is infinitely long in only one direction, either downstream or upstream. But solutions in which a semi-infinite tube has multiple neckings or swellings do not exist. For finite-length tubes, there exist 'pieces' of both swelling and necking solitary waves, as well as close-to-solitary-wave solutions with a finite number of successive swellings or neckings.

The principal point of constructing a solution in an infinitely long tube conveying a viscous fluid is the existence of a limited material stretch that reflects the limited extensibility of polymeric molecular chains, which is a principal feature of Gent material (Gent, 1996; Horgan, 2015). For other conventional hyperelastic models, such as Ogden material, there is no limited stretch so that the tube will infinitely swell upstream and narrow downstream. However, for realistic fluid viscosity, the difference in the tube's limit behaviour will manifest itself at thousands of diameters upstream and downstream from the central segment so that for practical applications, the results of the present study can be transferred to other hyperelastic rubber models without any changes.

Finally, we note that the stability of the obtained solutions is not analysed in this study, and this could be a topic of a separate investigation.

Declaration of competing interest

The authors declare that they have no known competing financial interests or personal relationships that could have appeared to influence the work reported in this paper.

Acknowledgements

I thank A.T. Il'ichev for stimulating discussions on the problem. This work was supported by a grant of the Russian Foundation for Basic Research No. 18-29-10020.

References

Alhayani, A.A., Rodríguez, J., Merodio, J., 2014. Numerical analysis of neck and bulge propagation in anisotropic tubes subject to axial loading and internal pressure. Finite Elem. Anal. Des. 10, 11–19.

Amabili, M., Balasubramanian, P., Bozzo, I., Breslavsky, I.D., Ferrari, G., Franchini, G., Giovanniello, F., Pogue, C., 2020. Nonlinear dynamics of human aortas for material characterization. Phys. Rev. X 10, 011015.

Anand, M., Rajagopal, K.R., 2004. A shear-thinning viscoelastic blood model for describing the flow of blood. Int. J. Cardiovasc. Med. Sci. 32, 601–608.

Breslavsky, I.D., Amabili, M., Legrand, M., 2016. Static and dynamic behavior of circular cylindrical shell made of hyperelastic arterial material. J. Appl. Mech. 83 (5), 051002.

Cao, Y., Zheng, Y., Li, G.-Y., Jiang, Y., 2019. Elastodiagnosis of diseases: A review. Extreme Mech. Lett. 27, 102–123.

de Gelidia, S., Bucchia, A., 2019. Comparative finite element modelling of aneurysm formation and physiologic inflation in the descending aorta. Comput. Methods Biomech. Biomed. Eng. 22 (15), 1197–1208.

Dehghani, H., Desena-Galarza, D., Jha, N.K., Reinoso, J., Merodio, J., 2019. Bifurcation and post-bifurcation of an inflated and extended residually-stressed circular cylindrical tube with application to aneurysms initiation and propagation in arterial wall tissue. Finite Elem. Anal. Des. 161, 51–60.

Demiray, H., 1996. Solitary waves in prestressed elastic tubes. Bull. Math. Biol. 58 (5), 939–955.

Epstein, M., Johnston, C.R., 2001. On the exact speed and amplitude of solitary waves in fluid-filled elastic tubes. Proc. R. Soc. Lond. Ser. A Math. Phys. Eng. Sci. 457, 1195–1213.

Fu, Y.B., Il'ichev, A.T., 2010. Solitary waves in fluid-filled elastic tubes: existence, persistence, and the role of axial displacement. IMA J. Appl. Math. 75, 257–268.

Fu, Y.B., Il'ichev, A.T., 2015. Localized standing waves in a hyperelastic membrane tube and their stabilization by a mean flow. Math. Mech. Solids 20, 1198–1214.

Fu, Y.B., Pearce, S.P., Liu, K.K., 2008. Post-bifurcation analysis of a thin-walled hyperelastic tube under inflation. Int. J. Non-Linear Mech. 43, 697–706.

Fu, Y.B., Xie, Y.X., 2012. Effects of imperfections on localized bulging in inflated membrane tubes. Philos. Trans. R. Soc. A 370, 1896–1911.

Galdi, G.P., Rannacher, R., Robertson, A.M., Turek, S., 2008. Hemodynamical Flows. Modeling, Analysis and Simulation. Birkhäuser Verlag.

Gent, A.N., 1996. A new constitutive relation for rubber. Rubber Chem. Technol. 69, 59–61.

Gijsen, F.J.H., van de Vosse, F.N., Janssen, J.D., 1999. The influence of the non-Newtonian properties of blood on the flow in large arteries: steady flow in a carotid bifurcation model. J. Biomech. 32, 601–608.

Grotberg, J.B., Jensen, O.E., 2004. Biofluid mechanics in flexible tubes. Ann. Rev. Fluid Mech. 36, 121–147.

Guo, Z., Wang, S., Li, L., Ji, H., Wang, Z., Cai, S., 2014. Inflation of stressed cylindrical tubes: An experimental study. Proc. SPIE 9234, 92340H.

Heil, M., Hazel, A.L., 2011. Fluid-structure interaction in internal physiological flows. Ann. Rev. Fluid Mech. 43, 141–162.

Horgan, C.O., 2015. The remarkable Gent constitutive model for hyperelastic materials. Int. J. Non-Linear Mech. 68, 9–16.

Il'ichev, A.T., Fu, Y.B., 2012. Stability of aneurysm solutions in a fluid-filled elastic membrane tube. Acta Mech. Sinica 28 (4), 1209–1218.

Il'ichev, A.T., Fu, Y.B., 2014. Stability of an inflated hyperelastic membrane tube with localized wall thinning. Int. J. Eng. Sci. 80, 53–61.

Il'ichev, A.T., Shargatov, V.A., Fu, Y.B., 2020. Characterization and dynamical stability of fully nonlinear strain solitary waves in a fluid-filled hyperelastic membrane tube. Acta Mech. (accepted).

Jensen, O.E., 1990. Instabilities of flow in a collapsed tube. J. Fluid Mech. 220, 623–659.

Jensen, O.E., Pedley, T.J., 1989. The existence of steady flow in a collapsed tube. J. Fluid Mech. 206, 339–374.

Karagiozis, K.N., Paidoussis, M.P., Amabili, M., 2007. Effect of geometry on the stability of cylindrical clamped shells subjected to internal fluid flow. Comput. Struct. 85, 645–659.

Ku, D.N., 1997. Blood flow in arteries. Annu. Rev. Fluid Mech. 29, 399–434.

Kyriakides, S., Chang, Y.-C., 1991. The initiation and propagation of a localized instability in an inflated elastic tube. Int. J. Solids Struct. 27, 1085–1111.

Metzner, A.B., Reed, J.C., 1955. Flow of non-Newtonian fluids-correlation of the laminar, transition, and turbulent-flow regions. AIChE J. 1 (4), 434–440.

Moore, Jr., J.E., Maier, S.E., Ku, D.N., Boesiger, P., 1985. Hemodynamics in the abdominal aorta: a comparison of in vitro and in vivo measurements. J. Appl. Physiol. 76 (4), 1520–1527.

Pamplona, D.C., Goncalves, P.B., Lopes, S.R.X., 2006. Finite deformations of cylindrical membrane under internal pressure. Int. J. Mech. Sci. 48, 683–696.

Pearce, S.P., Fu, Y.B., 2010. Characterization and stability of localized bulging/necking in inflated membrane tubes. IMA J. Appl. Math. 75, 581–602.

Pedley, T.J., 2003. Arterial and venous fluid dynamics. In: Pedrizzetti, G., Perktold, K. (Eds.), Cardiovascular Fluid Mechanics. Springer, pp. 1–72 (Chap. 1).

Pedley, T.J., Luo, X.Y., 1998. Modelling flow and oscillations in collapsible tubes. Theor. Comput. Fluid Dyn. 10, 277–294.

Poroshina, A.B., Vedeneev, V.V., 2018. Existence and uniqueness of steady state of elastic tubes conveying power law fluid. Russ. J. Biomech. 22 (2), 169–193.

Vassilevski, Yu.V., Salamatova, V.Yu., Simakov, S.S., 2015. On the elasticity of blood vessels in one-dimensional problems of hemodynamics. Comput. Math. Math. Phys. 55 (9), 1567–1578.

Vedeneev, V.V., Poroshina, A.B., 2018. Stability of an elastic tube conveying a non-Newtonian fluid and having a locally weakened section. Proc. Steklov Inst. Math. 300, 34–55.

Wang, S., Guo, Z., Zhou, L., Li, L., Fu, Y., 2019. An experimental study of localized bulging in inflated cylindrical tubes guided by newly emerged analytical results. J. Mech. Phys. Solids 124, 536–554.

Whittaker, R.J., Heil, M., Jensen, O.E., Waters, S.L., 2010. Predicting the onset of high-frequency self-excited oscillations in elastic-walled tubes. Proc. R. Soc. Lond. Ser. A Math. Phys. Eng. Sci. 466, 3635–3657.

Yomosa, S., 1987. Solitary waves in large blood vessels. J. Phys. Soc. Japan 56 (2), 506–520.

Yushutin, V.S., 2012. Stability of flow of a nonlinear viscous power-law hardening medium in a deformable channel. Moscow Univ. Mech. Bull. 67 (4), 99–102.